

PAPER • OPEN ACCESS

Non-linear magnetotropic susceptibility in FePS₃

To cite this article: Hamza Farooq and Muhammad Nauman 2025 *J. Phys.: Condens. Matter* **37** 405801

View the article online for updates and enhancements.

You may also like

- Imprint of inflation on galaxy shape correlations
 Fabian Schmidt, Nora Elisa Chisari and Cora Dvorkin
- Mixing and turbulent mixing in fluids, plasma and materials: summary of works presented at the 3rd International Conference on Turbulent Mixing and Beyond Serge Gauthier, Christopher J Keane, Joseph J Niemela et al.
- First International Workshop on Nonequilibrium Processes in Plasma Physics and Studies of Environment Z Lj Petrovi, G Malovi, M Tasi et al.

J. Phys.: Condens. Matter 37 (2025) 405801 (9pp)

https://doi.org/10.1088/1361-648X/ae0913

Non-linear magnetotropic susceptibility in FePS₃

Hamza Farooq¹ and Muhammad Nauman^{1,2,*}

- ¹ Department of Physics and Astronomy, National University of Sciences and Technology (NUST), Islamabad 44000, Pakistan
- ² Institute of Science and Technology Austria (ISTA), Klosterneuburg 3400, Austria

E-mail: nouman.kakakhail@gmail.com

Received 23 May 2025, revised 19 August 2025 Accepted for publication 17 September 2025 Published 30 September 2025



Abstract

Magnetotropic susceptibility is the thermodynamic coefficient that maps the curvature of free energy with respect to an applied magnetic field orientation, providing a means to quantify the magnetic anisotropy of a crystal. In this context, non-linear magnetic torque behavior has been reported in FePS₃, motivating the investigation of similar non-linear characteristics in its magnetotropic susceptibility. In this work, we derive the non-linear magnetotropic susceptibility expressions for FePS₃ in both ac^* -and bc^* -planes using complementary approaches: by taking the first derivative of torque and through the formal calculation of the magnetotropic susceptibility. Higher-order terms in the magnetization are included, and the final equations are obtained by applying symmetry constraints imposed by the C_{2h} point group of the material. We analyze the behavior of the resulting non-linear expressions and identify the contributions of each parameter. Our theoretical results show good agreement with preliminary, unpublished experimental data, offering meaningful guidance for ongoing and future experimental work.

Keywords: magnetotropic, susceptibilities, FePS₃

1. Introduction

Two-dimensional (2D) materials have attracted significant attention due to the emergence of novel physical phenomena driven by their reduced dimensionality. Among these, magnetism in 2D has been a 'talk of the town' since the discovery of graphene, offering prospects for next-generation spintronics, magnonics, and quantum devices [1–4]. In particular, the study of 2D materials with magnetic ordering is expected to facilitate the development of spintronic devices and water purification for clean water research. A key subclass of these

* Author to whom any correspondence should be addressed.

Original content from this work may be used under the terms of the Creative Commons Attribution 4.0 licence. Any further distribution of this work must maintain attribution to the author(s) and the title of the work, journal citation and DOI.

materials is the layered transition metal (TM) trichalcogenides (TMPS₃, TM = Fe, Co, Mn, V, Zn, or Ni), where weak van der Waals bonding between layers permits mechanical or chemical exfoliation down to monolayers, enabling the exploration of true 2D magnetic behavior [1, 5–12]. These compounds' honeycomb structure comprises TM atoms/ions, each connected to six trigonal-symmetric sulfur atoms. A dumbbell structure is created when the sulfur atoms connect with two phosphorus atoms, one above and one below the honeycomb structure. Although all these compounds are isostructural and the magnetic lattice has the 2D honeycomb structure [13], their spin dimensionalities differ. For example, for FePS₃ and MnPS₃, the magnetization axis is perpendicular to the layers, while for NiPS₃ it lies in the plane of the layers in the ordered state. The spin dimensionality of FePS₃, NiPS₃, and MnPS₃ corresponds to the Ising type, XY (or XXZ) type, and Heisenberg-type AFM systems, respectively [12]. In the paramagnetic regime, while the susceptibility of MnPS3 is isotropic and that of NiPS3 is weakly anisotropic, FePS3 exhibits highly anisotropic susceptibility. In this regard, new tools and techniques could pave the way for an in-depth understanding of these materials for fundamental physics and advancing their potential use in spintronic applications.

FePS₃ offers an interesting platform for symmetry-driven physics. For example, a recently reported metastable magnetization state induced by nonlinear terahertz spectroscopy reveals a change in the free energy landscape. The symmetric free energy response in the absence of a specific phonon mode excitation changes into an asymmetric shape after the phonon mode is excited [14]. This signals towards the emergent states induced by nonlinear physics having ties with the structural properties and hence demands the mapping of free energy curvature in the nonlinear regime.

Recent torque magnetometry studies show non-linear behavior in both angle and magnetic field dependent torque signal. The theoretical calculations successfully captured the key features of the experimental torque behavior, considering non-linearity in the off-diagonal elements of the magnetic susceptibility tensor [15]. However, the systematic inclusion of non-linearity in magnetization and susceptibility and its effect on the free energy landscape are interesting areas to explore.

In this paper, a recently reported technique, resonant torsion magnetometry [16], is used to study the Ising antiferromagnet FePS₃. This technique measures the magnetotropic susceptibility, a thermodynamics coefficient equivalent to the curvature of free energy with respect to applied magnetic field orientation $(k = \frac{\partial^2 F}{\partial \theta^2})$. This technique has been employed for RuCl₃ in search of a quantum spin liquid state [17]. The complicated interactions in RuCl₃, such as Kitaev, Gamma, and Ising exchange, make it hard to explicitly study the AFM Ising interaction and the role of monoclinic structure in magnetic properties. FePS₃ is isostructural with RuCl₃ and provides an interesting platform for exploring the magnetic behavior entangled with structural properties, thanks to its strong magnetoelastic coupling [18-20]. By calculating the magnetotropic susceptibility [21], we provide some results reporting how this quantity can be derived from the first derivative of torque, and where considering the correct magnetotropic equation from [21] is inevitable. We study how the magnetotropic coefficient (k) behaves under linear and nonlinear regimes by simplifying the magnetotropic equations using symmetry and group theoretical considerations arising from the monoclinic crystal structure and the C_{2h} symmetry of FePS₃.

2. Results and discussion

Figure 1 shows the positions of the Fe atoms in the crystal structure for three different planes with the corresponding angle definitions following the same arrangement as given in [15], where the ab-plane corresponds to the hard plane while the c^* -axis corresponds to the easy axis perpendicular to the plane. The c index refers to the c^* -axis and not to the crystallographic c-axis unless otherwise stated.

To understand the implications of structure on the magnetic properties, we use the magnetotropic susceptibility, which is proportional to the magnetic susceptibility (χ) . It is the second derivative of free energy (F), or first derivative of torque, with respect to magnetic field angle $k = \partial \tau / \partial \theta = \partial^2 F / \partial \theta^2$ [21] where θ is the angle between the magnetic field and c^* -axis. It is defined in [21] as,

$$k = (\mathbf{n} \times \mathbf{B}) \cdot (\mathbf{n} \times \mathbf{M}) - (\mathbf{n} \times \mathbf{B}) \cdot \mathbf{\chi} (\mathbf{B}) \cdot (\mathbf{n} \times \mathbf{B})$$
 (1)

where n is the axis of rotation, B is the external magnetic field [16, 21], M is the magnetization, and χ is the magnetic susceptibility. The magnetization and magnetic susceptibility are related via $M_i = \chi_{ij}B_j$ or $\chi_{ij} = \frac{\partial M_i}{\partial B_j}$ where i, j, k, are the coordinate axes defined when picking a frame of reference. In our case, these are the a-, b-, and c^* -axes.

In the linear regime, the magnetization (M) is linearly proportional to the magnetic field (B), while the linear magnetic susceptibility (χ^0_{ij}) remains independent of the magnetic field (B). We can use equation (1) to obtain the linear magnetotropic susceptibility equations, only considering the diagonal magnetic susceptibility tensor, in the principal crystal directions for magnetic susceptibility. Alternatively, magnetotropic susceptibility is also defined as the slope of torque $(k = \frac{\partial \tau}{\partial \theta})$. So, we can arrive at the magnetotropic susceptibility equations by differentiating the equations for torque from [15],

$$k_{ac}(\theta) = (\chi_{cc} - \chi_{aa})B^2\cos(2\theta)$$
 for $\phi = 0^{\circ}$ (2a)

$$k_{bc}(\theta) = (\chi_{cc} - \chi_{bb}) B^2 \cos(2\theta) \text{ for } \phi = 90^{\circ}$$
 (2b)

where χ_{aa} , χ_{bb} , χ_{cc} are considered as the principal magnetic susceptibilities. The calculated curve from the above two equations has the form shown in figure 2(a). where a clear $\cos(2\theta)$ dependence indicates a linear response regime where $k \propto B^2$ is evident from figure 2(b). We do not show k_{bc} curves since $k_{bc} \approx k_{ac}$ considering isotropic behavior in the ab-plane from reported SQUID measurements [19].

The plots in figure 2 resemble those of magnetic torque [15], with the peaks occurring along the principal axes rather than at 45°, a direct consequence of measuring the slope of the torque. This approach yields maximum amplitude along the principal crystal axes, at least in the linear regime, unlike conventional torque measurements, which vanish along these directions.

In [15], the off-diagonal components of the magnetic susceptibility tensor are taken as non-linear where $\chi_{ca} = \chi_{ca}^0 B_c^2$ and $\chi_{ac} = \chi_{ac}^0 B_a^2$, which modifies the torque in the *ac*-plane as,

$$au_{ac} = rac{1}{2} \left(\chi_{cc} - \chi_{aa} \right) B^2 \sin(2\theta) + rac{1}{4} \left(\chi_{ca}^0 - \chi_{ac}^0 \right) B^4 \sin^2(2\theta) \,.$$

The theoretically calculated curves from this equation nicely reconcile with the experimentally measured torque curves as reported in [15]. We can arrive at an equation for

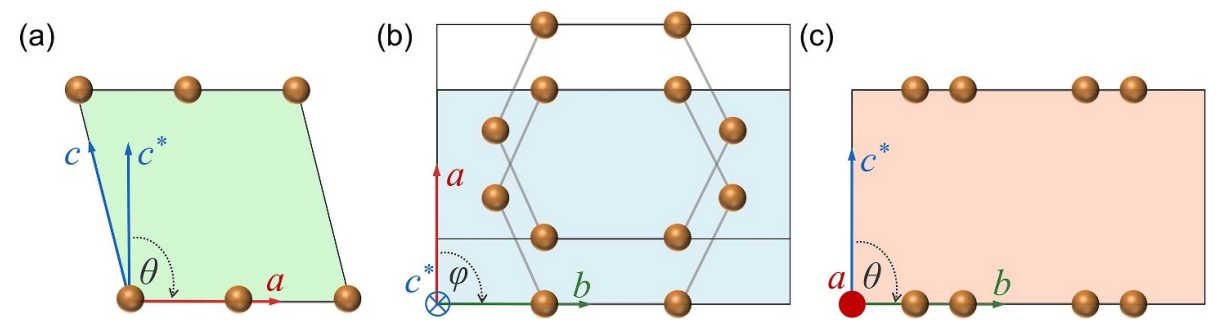


Figure 1. An overview of the crystal structure of FePS₃ with only Fe atoms by looking from (a) b-axis, (b) c^* -axis (perpendicular to the ab-plane), and (c) a-axis (arrows not to scale).

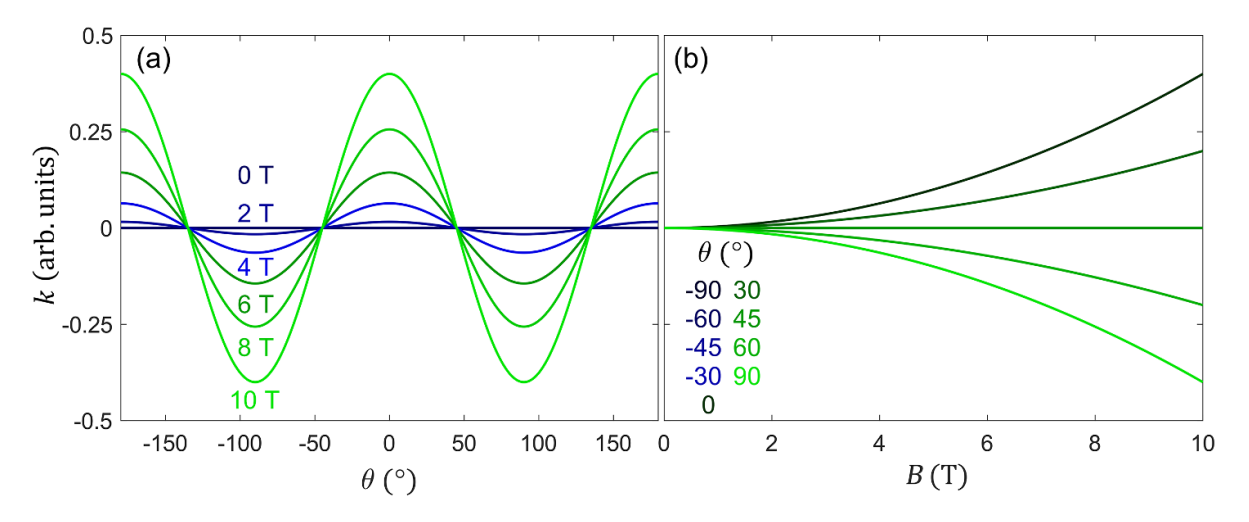


Figure 2. (a) Plot of k vs θ , (b) k vs magnetic field B where $\Delta \chi = 0.004$ emu · mol⁻¹ · Oe⁻¹. Data for χ taken from [15].

magnetotropic susceptibility by differentiation of the above χ in its complete form in the linear regime, represented as: equation,

$$k_{ac}^{(\tau)} = \frac{\partial \tau_{ac}}{\partial \theta} = (\chi_{cc} - \chi_{aa}) B^2 \cos(2\theta) + \frac{1}{2} (\chi_{ca}^0 - \chi_{ac}^0) B^4 \sin(4\theta).$$
 (3)

The obtained calculated curve from equation (3) is shown in figure 3(a), which is compared with the available experimental curve shown in figure 3(b) [22]. Equation (3) cannot produce the features shown in figure 3(b) (see also figure A1 in the appendix). There is an apparent difference between the nonlinear curve obtained from torque and experimental results. Hence, we conduct a systematic derivation for the non-linear magnetotropic equation using equation (1). In what follows, we study the behavior of k as the off-diagonal components are introduced in the ac^* -plane (same as the ac-plane), i.e. considering that the a- and c^* - axes may not be the principal axes for magnetic susceptibility. Furthermore, we derive the form of the non-linear term by considering the expansion of the magnetization in terms of the magnetic field. Before proceeding with the formal expansion of the magnetization and magnetic susceptibility, we consider a full magnetic susceptibility tensor

$$\chi = \left[\begin{array}{ccc} \chi_{aa} & \chi_{ab} & \chi_{ac} \\ \chi_{ba} & \chi_{bb} & \chi_{bc} \\ \chi_{ca} & \chi_{cb} & \chi_{cc} \end{array} \right]$$

where we remind the reader that the c index corresponds to the easy c^* -axis and not to the crystallographic c-axis.

To properly consider the susceptibility tensor that respects the symmetry of the crystal, we resort to the crystal structure of FePS₃, which has a broken mirror symmetry in the ac*plane, shown in figure 1(a), which comes from the monoclinic structure of the crystal. Taking account of this symmetry, we are left with the following,

$$\chi' = \begin{bmatrix} \chi_{aa} & 0 & \chi_{ac} \\ 0 & \chi_{bb} & 0 \\ \chi_{ca} & 0 & \chi_{cc} \end{bmatrix}.$$

Solving equation (1) for this complete magnetic susceptibility tensor and the ac^* -plane of rotation (i.e. n = b) where the magnetic field vector is confined to the ac-plane of rotation

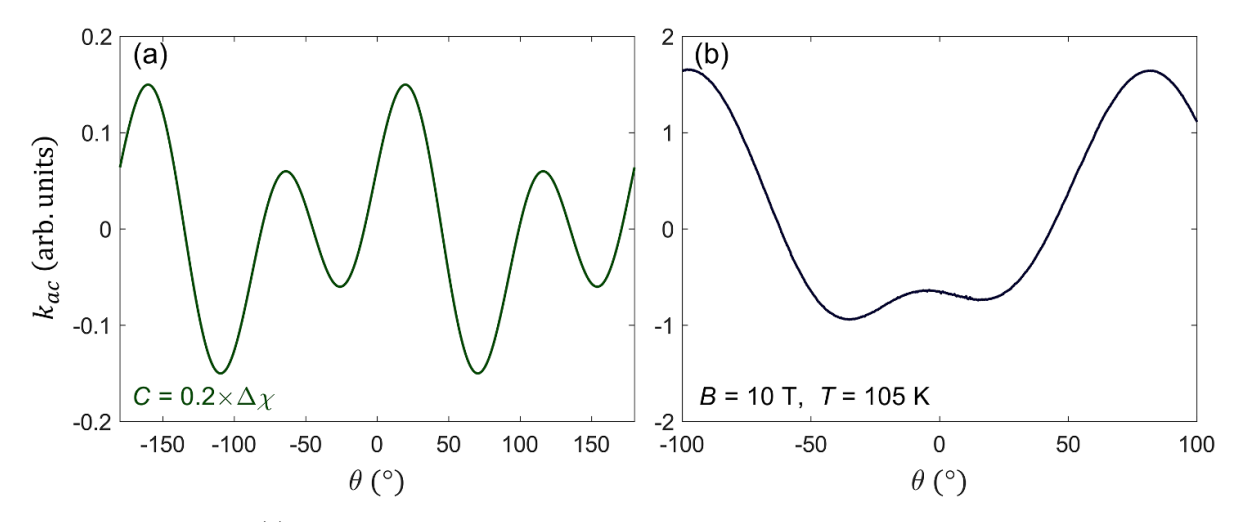


Figure 3. (a) Sample curve of $k_{ac}^{(\tau)}$ (equation (3)) where $C = \frac{1}{2} \left(\chi_{ca}^0 - \chi_{ac}^0 \right) = 0.2 \Delta \chi$ at B = 4 T and $\Delta \chi = 0.004$ emu · mol⁻¹ · Oe⁻¹ (b) Experimentally measured curve at T = 105 K and B = 10 T [22].

$$(\vec{B} = (B_a \quad 0 \quad B_c))$$
 gives,

$$k_b(\theta, \mathbf{B}) = (\chi_{cc} - \chi_{aa})B^2 \cos(2\theta) + (\chi_{ac} + \chi_{ca})B^2 \sin(2\theta).$$
(4)

Plotting the above equation provides clear information on the role of off-diagonal magnetic susceptibility elements. The trend has been explored for different values of the diagonal $(\Delta\chi=\chi_{cc}-\chi_{aa})$ and off-diagonal susceptibilities $(\chi_{ac}+\chi_{ca}=2\chi_{ca})$, which appear as the coefficients of the $\cos{(2\theta)}$ and $\sin{(2\theta)}$ terms in the above equation, respectively.

Figure 4 shows that the curve's peak appears along the principal axis (dark blue curve) in the absence of the magnetic susceptibility tensor's off-diagonal elements $(2\chi_{ca}=0)$. The peak gradually shifts along the θ -axis as the contributions from the off-diagonal elements are switched on and increased progressively to half, equal, three halves, twice, and five halves the value of the amplitude $(\Delta\chi)$ as shown in figure 4, with a red dashed arrow as a guide to the eye. This is what is expected from the $\sin{(2\theta)}$ term of equation (3) that causes a peak shift due to the non-zero off-diagonal susceptibility elements while also contributing towards the magnitude of the peaks. Hence, we identify the peak shift as a marker of deviation from the principal axis configuration. This shift arises from the off-diagonal susceptibility elements when the experimental geometry is misaligned with the true principal axes.

So far, we have only considered the linear response regime where the magnetization grows linearly with the applied magnetic field ($M_i = \chi_{ij}B_j$). We now consider the natural extension to the linear regime by adding terms proportional to higher powers of B in the magnetization. This will give us the higher-order term in the magnetotropic equation. We start with the expansion of magnetization to higher-order terms,

$$M_i = m_{ij}^{(1)} B_j + m_{ijk}^{(2)} B_j B_k + m_{ijkl}^{(3)} B_j B_k B_l + \dots$$

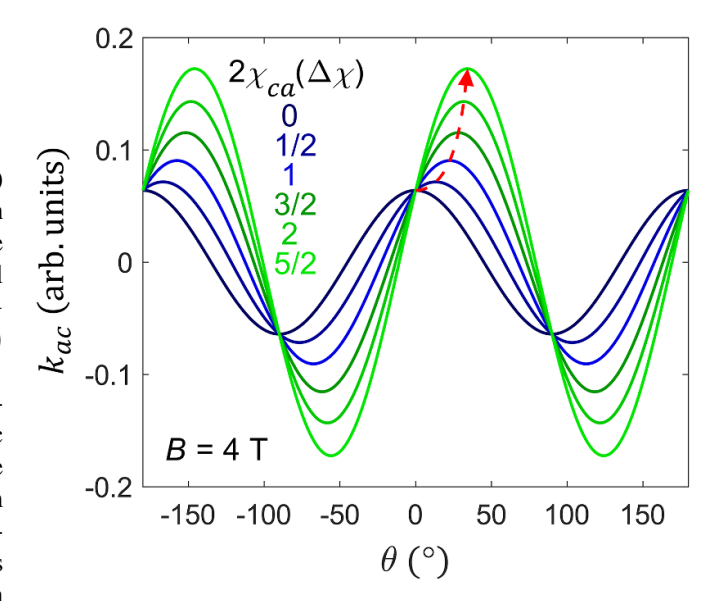


Figure 4. A plot of k vs. θ considering the full linear magnetic susceptibility tensor in the ac-plane of rotation for the sum of the off-diagonal susceptibility equal to $0, \frac{1}{2}\Delta\chi, \Delta\chi, \frac{3}{2}\Delta\chi, 2\Delta\chi, \frac{5}{2}\Delta\chi$ in the units of emu·mol⁻¹·Oe⁻¹ at B=4 T. The Red dashed arrow is a guide to the eye.

Since the crystal is centrosymmetric, we require that $m_{ijk}^{(2)} = 0$. Whence,

$$M_i = m_{ii}^{(1)} B_i + m_{iikl}^{(3)} B_i B_k B_l.$$

We only retain two terms. It can also be shown that $m^{(1)}$ is the linear magnetic susceptibility tensor $\chi^{(0)}$ and $m^{(3)}_{ijkl} = \frac{1}{3!}\chi^{(2)}_{ijkl}$ is a fourth rank tensor having 81 components, where $\chi^{(2)}_{ijkl} = \left(\frac{\partial^3 M_i}{\partial B_j \partial B_k \partial B_l}\right)\Big|_{B=0}$.

The fourth rank tensor $m_{ijkl}^{(3)}$ can be taken as symmetric with respect to any permutation of j, k, and l due to its contraction

with $B_j B_k B_l$. Furthermore, using energy considerations, we can show that $m_{ijkl}^{(3)}$ is also symmetric in the exchange of the i index. Hence, we may take $m_{ijkl}^{(3)}$ to be symmetric in all four indices,

$$m_{ijkl}^{(3)} = m_{jikl}^{(3)} = m_{jkil}^{(3)} = m_{kilj}^{(3)} = \dots$$

This reduces the number of independent components to 15. Due to the C_2^b rotation symmetry, only even combinations of b indices are allowed, further reducing the number of independent components to 9. This exhausts all the constraints enforced by the crystal symmetry. With the expansion of M, the equation for magnetotropic susceptibility becomes,

$$k_{n}(B) = (n \times B) \cdot \left(n \times \left(M^{(0)} + M^{(1)}\right)\right)$$
$$- (n \times B) \cdot \left(\chi^{(0)} + \chi^{(1)}\right) \cdot (n \times B).$$

Where $M_i^{(0)} = m_{ij}^{(1)} B_j$, $M_i^{(1)} = m_{ijkl}^{(3)} B_j B_k B_l$, $\chi_{\mu\nu}^{(0)} = m_{\mu\nu}^{(1)}$, and $\chi_{\mu\nu}^{(1)} = 3m_{\mu\nu kl}^{(3)} B_k B_l$. In the last case, we have used $\chi_{\mu\nu} = \frac{\partial M_{\mu}}{\partial B_{\nu}}$ from which we have $\chi_{\mu\nu}^{(1)} = \frac{\partial M_{\mu}^{(1)}}{\partial B_{\nu}}$. After separating the linear and non-linear terms, we arrive at,

$$k_n(B) = k_n^{(0)}(B) + k_n^{(1)}(B).$$
 (5)

Where,

$$k_{n}^{(0)}(B) = (n \times B) \cdot \left(n \times \left(M^{(0)}\right)\right)$$

$$- (n \times B) \cdot \left(\chi^{(0)}\right) \cdot (n \times B) \qquad (6a)$$

$$k_{n}^{(1)}(B) = (n \times B) \cdot \left(n \times \left(M^{(1)}\right)\right)$$

$$- (n \times B) \cdot \left(\chi^{(1)}\right) \cdot (n \times B). \qquad (6b)$$

Elaborating equation (6b) in the ac^* -plane (or ac-plane) results in,

$$\begin{split} k_{ac}^{(1)}\left(B\right) &= \left(10m_{aaac}^{(3)} - 6m_{ccca}^{(3)}\right)B_{a}^{3}B_{c} \\ &+ \left(18m_{ccaa}^{(3)} - 3m_{aaaa}^{(3)} - 3m_{ccc}^{(3)}\right)B_{a}^{2}B_{c}^{2} \\ &+ \left(10m_{ccca}^{(3)} - 6m_{aaac}^{(3)}\right)B_{c}^{3}B_{a} + \left(m_{aaaa}^{(3)} - 3m_{ccaa}^{(3)}\right)B_{a}^{4} \\ &+ \left(m_{ccc}^{(3)} - 3m_{ccaa}^{(3)}\right)B_{c}^{4}. \end{split}$$

And the full magnetotropic equation is of the form,

$$k_{ac}(B) = (\chi_{cc} - \chi_{aa}) B^{2} \cos(2\theta) + (\chi_{ac} + \chi_{ca}) B^{2} \sin(2\theta) + C_{ac} B^{4} \sin^{3}(\theta) \cos(\theta) + D_{ac} B^{4} \sin^{2}(\theta) \cos^{2}(\theta) + E_{ac} B^{4} \cos^{3}(\theta) \sin(\theta) + F_{ac} B^{4} \sin^{4}(\theta) + G_{ac} B^{4} \cos^{4}(\theta)$$
(7)

where $C_{ac} = 10 m_{aaac}^{(3)} - 6 m_{ccca}^{(3)}$, $D_{ac} = 18 m_{ccaa}^{(3)} - 3 m_{aaaa}^{(3)} - 3 m_{ccaa}^{(3)}$, $C_{ac} = 10 m_{ccca}^{(3)} - 6 m_{aaac}^{(3)}$, $C_{ac} = m_{aaaa}^{(3)} - 3 m_{ccaa}^{(3)}$, $C_{ac} = m_{ccc}^{(3)} - 3 m_{ccaa}^{(3)}$. We see from equation (7) that $C_{ac} = -3 (F_{ac} + G_{ac})$.

In the bc^* -plane, we get the same result as the ac^* -plane with index a replaced by index b. Hence,

$$\begin{split} k_{bc}^{(1)}\left(B\right) &= \left(10m_{bbbc}^{(3)} - 6m_{cccb}^{(3)}\right)B_b^3B_c \\ &+ \left(18m_{ccbb}^{(3)} - 3m_{bbbb}^{(3)} - 3m_{cccc}^{(3)}\right)B_b^2B_c^2 \\ &+ \left(10m_{cccb}^{(3)} - 6m_{bbbc}^{(3)}\right)B_c^3B_b + \left(m_{bbbb}^{(3)} - 3m_{ccbb}^{(3)}\right)B_b^4 \\ &+ \left(m_{cccc}^{(3)} - 3m_{ccbb}^{(3)}\right)B_c^4. \end{split}$$

However, only an even number of b indices are allowed. Causing the $B_c^3 B_b$ and $B_b^3 B_c$ terms to vanish,

$$\begin{aligned} k_{bc}^{(1)}\left(B\right) &= \left(18m_{ccbb}^{(3)} - 3m_{bbbb}^{(3)} - 3m_{ccc}^{(3)}\right)B_b^2B_c^2 \\ &+ \left(m_{bbbb}^{(3)} - 3m_{ccbb}^{(3)}\right)B_b^4 + \left(m_{ccc}^{(3)} - 3m_{ccbb}^{(3)}\right)B_c^4. \end{aligned}$$

And the complete equation in the bc^* -plane becomes,

$$k_{bc}(B) = (\chi_{cc} - \chi_{bb}) B^2 \cos(2\theta) + D_{bc} B^4 \sin^2(\theta) \cos^2(\theta) + F_{bc} B^4 \sin^4(\theta) + G_{bc} B^4 \cos^4(\theta).$$
 (8)

Where,
$$D_{bc} = 18m_{ccbb}^{(3)} - 3m_{bbbb}^{(3)} - 3m_{ccc}^{(3)}$$
, $F_{bc} = m_{bbbb}^{(3)} - 3m_{ccbb}^{(3)}$, $G_{bc} = m_{ccc}^{(3)} - 3m_{ccbb}^{(3)}$, $D_{bc} = -3(F_{bc} + G_{bc})$.

An alternate way of simplifying the magnetotropic

An alternate way of simplifying the magnetotropic equations $k_{ac}^{(1)}(B)$ and $k_{bc}^{(1)}(B)$ is using the symmetry properties of C_{2h} and its irreducible representations. The components of the total magnetic field (\vec{B}) reduce inside a FePS₃ crystal and transform in a way that respects crystal symmetry, as shown in table A1 (appendix).

In the C_{2h} group, B_b transforms as A_g , whereas B_a and B_c transform as B_g . The multiplication table for these irreducible representations is shown in table A2 (appendix).

We know that we have $k_n(B)$ on the left side of the equations, which has the dimension of energy, which is A_g in the language of irreducible representation. Hence, the terms on the right-hand side should have an identical representation required by the dimensional consistency of equations. The magnetic field (B) is an axial vector that is even under inversion. Due to this, the multiplication table (table A2) shows that the terms $B_b^3 B_c$ and $B_c^3 B_a$ will give an inconsistent representation (i.e. B_g) and hence are not allowed by the symmetry.

Plots of k_{bc} (equation (8)) are presented in figure 5(a). We see that G_{bc} characterizes the magnitude and sign of the central portion (easy axis), while F_{bc} characterizes the edges (hard plane). The wings are produced due to the D_{bc} term. There is a point of intersection between the curves at $\pm 30^{\circ}$ and $\pm 150^{\circ}$. A comparison with the linear curves (figure 2) shows that the period is still 180° with the curves being symmetrical about 0°. The inclusion of the non-linear terms results in the manifestation of additional peaks or wings not found in the linear case. The same remarks could be repeated in the case of k_{ac} due to the formal similarity of the coefficients, i.e., D_{ac} and D_{bc} , F_{ac} and F_{bc} , G_{ac} , and G_{bc} . Figure A2 (appendix) shows the curve behavior for different values of coefficients F_{bc} and G_{bc} .

In figure 5(b), we have plotted equation (7) where we have chosen $\chi_{ac} + \chi_{ca} = 0$ since we wish to capture the non-linear

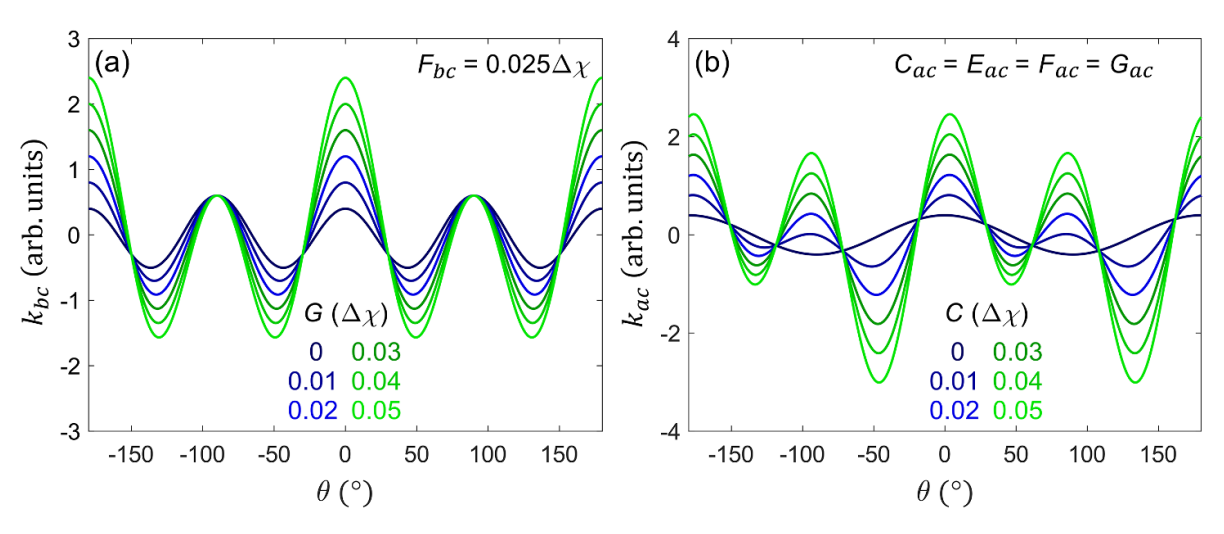


Figure 5. Plots of k vs θ for B=10 T, $\Delta\chi=0.004$ emu·mol⁻¹·Oe⁻¹. (a) Variation of k_{bc} at $F_{bc}=0.025\Delta\chi$ as G_{bc} is changed to see its effect on k_{bc} . (b) Variation of k_{ac} with all coefficients being equal.

behavior. We can see that the curve becomes asymmetric at about 0° . Variations due to C_{ac} and E_{ac} can be seen explicitly in figure A3. Figure A3 (a) shows the dependence of k_{ac} on the C_{ac} term. The peaks at 0° and $\pm 180^{\circ}$ remain fixed, whereas the peaks at $\pm 90^{\circ}$ shift to the left, gradually approaching 60° and -120° . The left wing progressively moves towards -60° while increasing in magnitude, whereas the right wing moves towards 0° while shrinking. In figure A3 (b), we look at the E_{ac} term. Here, the $\pm 90^{\circ}$ peaks are fixed while the central peak shifts to the right, gradually approaching 30° . The left wing moves towards -30° while still increasing in magnitude, and the right wing moves towards 90° while decreasing in magnitude

Figure A4 shows the behavior of k if we consider the nonlinear terms in isolation. From figure A4(a), we see the behavior of C; the region around 0° has a plateau, while the peaks occur at $\pm 60^\circ$ and $\pm 120^\circ$. In figures A4(b) and (d), the contribution of F and G to the region around the peaks at $\pm 90^\circ$ and 0°, respectively, can be seen. Figure A4(c) shows the behavior of the D term. It has a period of 90° compared with the rest of the terms, which, on the other hand, show a period of 180° . In the term involving E plotted in figure A4e, the plateau is around 90° while the peaks appear at $\pm 30^\circ$ and $\pm 150^\circ$.

Figure 6 presents the experimental magnetotropic susceptibility curve (black) measured at $T=105\,\mathrm{K}$ and $B=10\,\mathrm{T}$ [22], alongside the theoretical curve computed from our non-linear expression (equation (7)). The values of the coefficients used in the theoretical simulation are listed in table 1. Notably, the experimental curve exhibits key features predicted by the theoretical model, including the characteristic angular dependencies introduced by the non-linear terms. This qualitative agreement supports the validity of our symmetry-based approach. It suggests that the higher-order contributions we include play a meaningful role in the physical behavior of the system. While further experimental validation is needed, primarily through systematic measurements across different field strengths and

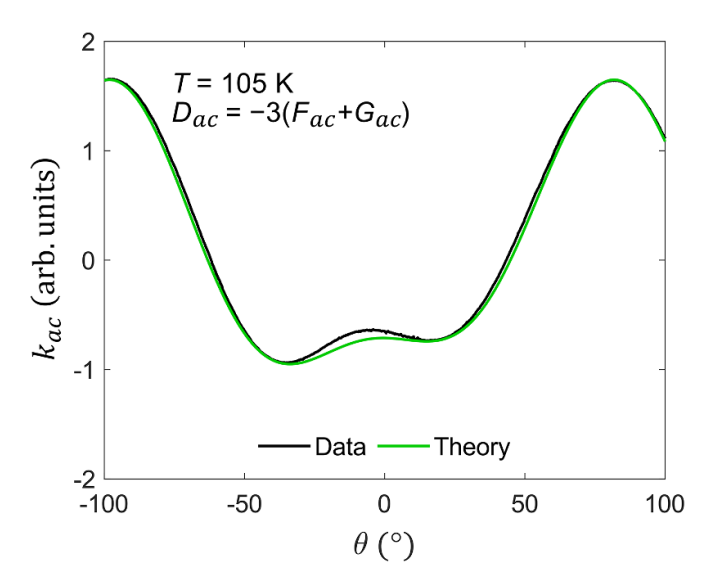


Figure 6. Comparison of the experimental [22] and theoretical curves (equation (7)) at $T = 105 \,\mathrm{K}$ and $B = 10 \,\mathrm{T}$.

Table 1. Fitting coefficients used in the theoretical curve in figure 6.

Co-efficient	Equivalent susceptibility	Value used
$\Delta \chi$	$\chi_{cc} - \chi_{aa}$	- 0.016
$2\chi_{ca}$	Off-diagonal $10m_{agac}^{(3)} - 6m_{ccca}^{(3)}$	$0.003 \\ 1.08 \times 10^{-4}$
E	$10m_{ccca}^{(3)} - 6m_{aaac}^{(3)}$	-6.19×10^{-5}
F	$m_{aaaa}^{(3)} - 3m_{ccaa}^{(3)}$	-7.28×10^{-6}
G	$m_{cccc}^{(3)}-3m_{ccaa}^{(3)}$	8.88×10^{-5}

temperatures, the observed alignment between theory and experiment offers promising initial confirmation and highlights the relevance of our phenomenological framework. We note that multiple parameter sets can produce similar fits if the linear terms are included as free parameters. To ensure stability, the linear terms should be fixed using data from the linear-response regime before fitting the nonlinear terms. A full specification of the fitting procedure is left for future work.

3. Conclusion

We have systematically calculated magnetotropic susceptibility using equations from the first derivative of torque [15] and proper derivation from the magnetotropic susceptibility equation [21]. The linear magnetotropic susceptibility equations agree with the linear torque curve except for a peak appearance at the principal crystallographic axis expected from the magnetotropic equation. In the linear regime, it was observed that the off-diagonal components of the magnetic susceptibility primarily result in a shift of the peak position, without significantly altering the overall shape of the curve.

The non-linear magnetotropic equation derived from the first derivative of torque exhibits behavior that deviates from the preliminary experimental curve. To address this discrepancy, we performed a more systematic derivation of the non-linear expression by expanding the magnetization to include higher-order terms. The isolated effect of each coefficient in the non-linear expression reveals features such as additional peaks and asymmetric shifts in the angular response. When compared with preliminary experimental results, the overall agreement with our phenomenological model is encouraging, indicating that the approach may be applicable to other systems exhibiting similar non-linear magnetic behavior.

We expect materials exhibiting magnetic exchange frustration, or more generally, systems with competing interactions, to show non-linear magnetotropic behavior. From an experimental standpoint, non-linear features may be more prominently detected in the temperature regimes where the linear magnetic susceptibilities tend to cancel each other. For FePS₃, this condition is more likely to be met in the vicinity of the magnetic phase transition, particularly around $T \approx 110$ K, making that temperature range promising for probing nonlinear magnetotropic effects. In this regime, high magnetic fields on the order of 10 T can also induce non-linear features, which we expect to appear in both magnetotropic susceptibility and angle-dependent torque measurements. Materials with low magnetic anisotropy may also meet the cancellation condition more readily, but they may have smaller non-linear coefficients, which could make detection more challenging. Thus, the relative suitability of low- and high-anisotropy systems remains an open question. Finally, we note that non-linear effects of the type discussed here may also arise in quadrupolar magnetotropic susceptibility measurements, where the free energy varies as the fourth power of the magnetic field.

4. Methods

The studies were performed by deriving the magnetotropic equations using torque equations [15] as a starting point. The same equations were counter-checked with equation (2) of [21]. The obtained equations were simulated using MATLAB and Mathematica. The magnetic susceptibility values were taken from [15].

Data availability statement

No new data were created or analysed in this study.

Acknowledgments

We thank Kimberly A. Modic for her support and discussions regarding the technique in the context of a project indirectly related to, but distinct from, the present work. We also thank Brad J. Ramshaw and Arkady Shekhter for scientific discussions not directly related to this study, but whose insights proved helpful. We are grateful to Valeska Zambra, Amit Nathwani, Hamza Nasir, and Tayyaba Hussain for informal discussions on various aspects of the technique, and to Naoya Iwahara for his thoughtful and constructive feedback. The experimental curve shown in figures 3(b) and 6, from the Thermodynamics of Quantum Materials (TQM) group at ISTA, was measured by Muhammad Nauman for an unrelated project. We thank Kimberly Modic for granting access to the laboratory facilities. Je Geun Park provided the crystal used for that measurement via Younjung Jo, whose contribution we gratefully acknowledge. Institutional support from the Institute of Science and Technology Austria (ISTA) is also gratefully acknowledged.

Author contributions

Hamza Farooq © 0009-0007-5494-6108 Formal analysis (equal), Investigation (equal), Methodology (equal), Writing – original draft (equal), Writing – review & editing (equal)

Muhammad Nauman © 0000-0002-2111-4846 Conceptualization (lead), Formal analysis (equal), Supervision (lead), Writing – review & editing (equal)

Appendix

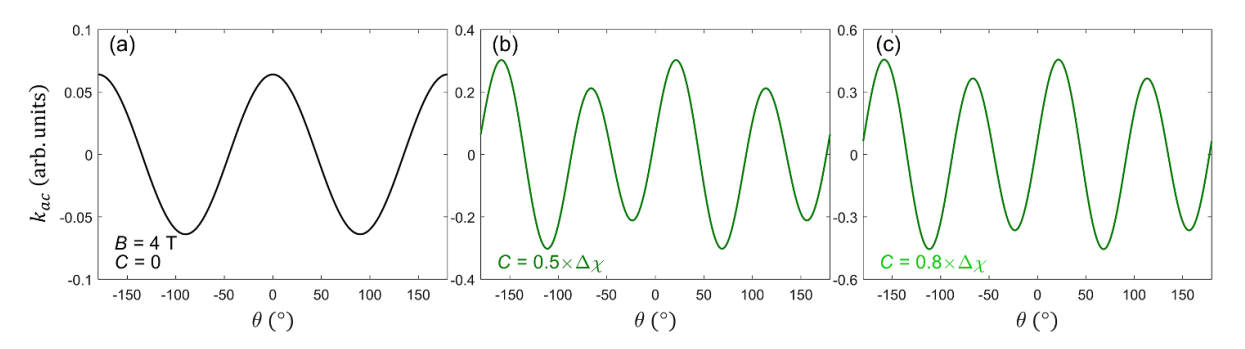


Figure A1. Variation of $k_{ac}^{(\tau)}$ (equation (3)) where $C=\frac{1}{2}\left(\chi_{ca}^{0}-\chi_{ac}^{0}\right)$ equal to (a) 0, (b) $0.5*\Delta\chi$ and (c) $0.8*\Delta\chi$ at B=4 T where $\Delta\chi=0.004$ emu \cdot mol $^{-1}\cdot$ Oe $^{-1}$.

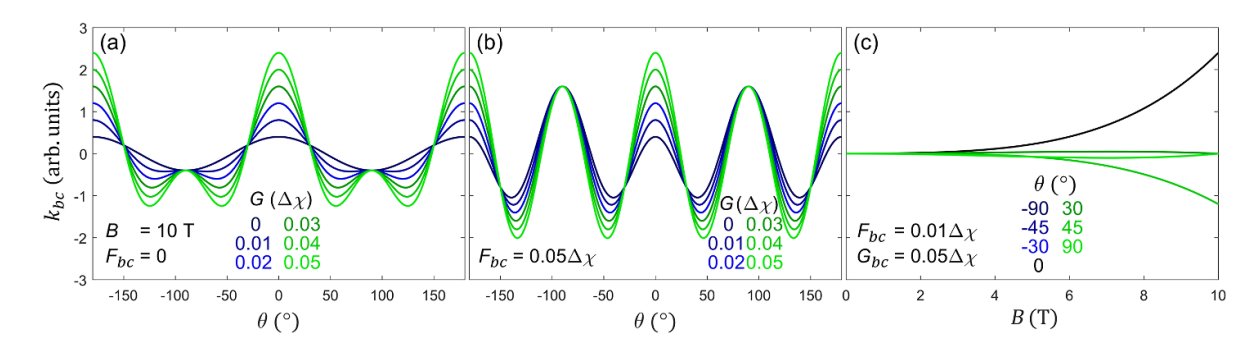


Figure A2. (a), (b) Angular spreads of k_{bc} for B=10 T, $\Delta\chi=0.004$ emu · mol $^{-1}$ · Oe $^{-1}$ (c) Response of k_{bc} with increasing field at various angles.

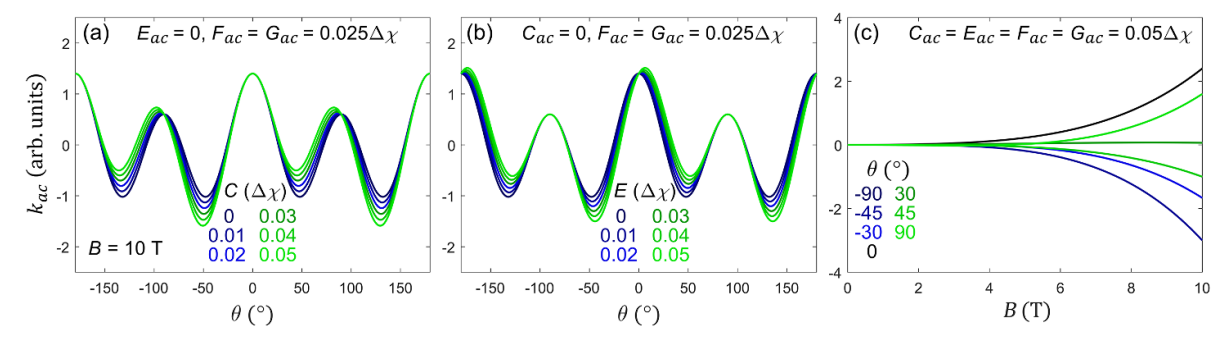


Figure A3. Plots of k_{ac} for B=10 T, $\Delta\chi=0.004$ emu · mol⁻¹ · Oe⁻¹. (a) Variation due to the C_{ac} term (b) Variation due to the E_{ac} term (c) Response of k_{ac} with increasing field at various angles.

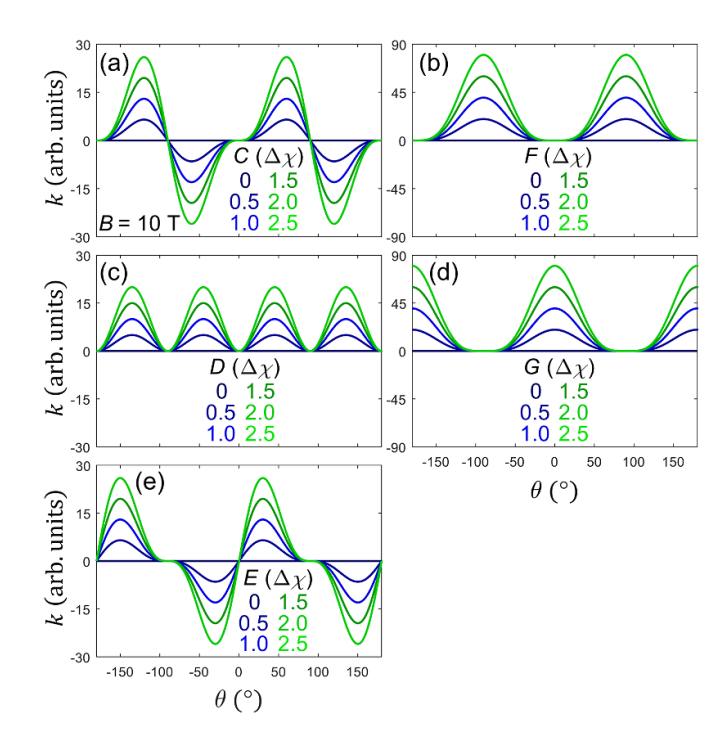


Figure A4. Plots of k vs. θ considering the terms in isolation. $\Delta \chi = 0.004 \; \mathrm{emu} \cdot \; \mathrm{mol}^{-1} \cdot \mathrm{Oe}^{-1}$ and $B = 10 \; \mathrm{T}$ for all the curves.

Table A1. A list of irreducible representations of the C_{2h} group.

C_{2h}	\vec{B} in C_{2h}	E	C_2	i	σ_h
A_g	B_b	1	1	1	1
B_g	B_a and B_c	1	-1	1	-1
A_u	_	1	1	-1	-1
B_u		1	-1	-1	1

Table A2. Multiplication table of C_{2h} group irreducible representation.

	A_g	B_g	A_u	B_u
A_g	A_g°	B_g	A_u	B_u
B_g	B_g	A_g	B_u	A_u
A_u	A_u	B_u	A_g	B_g
B_u	B_u	A_u	B_g	A_g

References

- [1] Park J-G 2016 Opportunities and challenges of 2D magnetic van der Waals materials: magnetic graphene? *J. Phys.* 28 301001
- [2] Gibertini M, Koperski M, Morpurgo A and Novoselov K 2019 Magnetic 2D materials and heterostructures *Nat. Nanotechnol.* 14 408–19
- [3] Susner M A, Chyasnavichyus M, McGuire M A, Ganesh P and Maksymovych P 2017 Metal thio-and selenophosphates as multifunctional van der waals layered materials Adv. Mater. 29 1602852

- [4] Wang F et al 2018 New frontiers on van der waals layered metal phosphorous trichalcogenides Adv. Funct. Mater. 28 1802151
- [5] Kuo C-T et al 2016 Exfoliation and Raman spectroscopic fingerprint of few-layer NiPS₃ van der Waals crystals Sci. Rep. 6 20904
- [6] Burch K S, Mandrus D and Park J-G 2018 Magnetism in two-dimensional van der Waals materials *Nature* 563 47
- [7] Tan C, Lee J, Jung S-G, Park T, Albarakati S, Partridge J, Field M R, McCulloch D G, Wang L and Lee C 2018 Hard magnetic properties in nanoflake van der Waals Fe₃GeTe₂ Nat. Commun. 9 1554
- [8] Lee S, Choi K-Y, Lee S, Park B H and Park J-G 2016 Tunneling transport of mono-and few-layers magnetic van der Waals MnPS₃ APL Mater. 4 086108
- [9] Kim S Y et al 2018 Charge-spin correlation in van der waals antiferromagnet NiPS₃ Phys. Rev. Lett. 120 136402
- [10] Wildes A et al 2015 Magnetic structure of the quasi-two-dimensional antiferromagnet NiPS₃ Phys. Rev. B 92 224408
- [11] Lancon D, Walker H C, Ressouche E, Ouladdiaf B, Rule K C, McIntyre G J, Hicks T J, Rønnow H M and Wildes A R 2016 Magnetic structure and magnon dynamics of the quasi-two-dimensional antiferromagnet FePS₃ Phys. Rev. B 94 214407
- [12] Kim K, Lim S Y, Lee J-U, Lee S, Kim T Y, Park K, Jeon G S, Park C-H, Park J-G and Cheong H 2019 Suppression of magnetic ordering in XXZ-type antiferromagnetic monolayer NiPS₃ Nat. Commun. 10 345
- [13] Chittari B L, Park Y, Lee D, Han M, MacDonald A H, Hwang E and Jung J 2016 Electronic and magnetic properties of single-layer MPX₃ metal phosphorous trichalcogenides *Phys. Rev. B* 94 184428
- [14] Ilyas B et al 2024 Terahertz field-induced metastable magnetization near criticality in FePS₃ Nature 636 609–14
- [15] Nauman M, Kiem D H, Lee S, Son S, Park J-G, Kang W, Han M J and Jo Y 2021 Complete mapping of magnetic anisotropy for prototype Ising van der Waals FePS₃ 2D Mater. 8 035011
- [16] Modic K A et al 2018 Resonant torsion magnetometry in anisotropic quantum materials Nat. Commun. 9 3975
- [17] Modic K A et al 2021 Scale-invariant magnetic anisotropy in RuCl₃ at high magnetic fields Nat. Phys. 17 240–4
- [18] Ergeçen E, Ilyas B, Kim J, Park J, Yilmaz M B, Luo T, Xiao D, Okamoto S, Park J-G and Gedik N 2023 Coherent detection of hidden spin-lattice coupling in a van der Waals antiferromagnet *Proc. Natl Acad. Sci.* 120 e2208968120
- [19] Wildes A, Lançon D, Chan M K, Weickert F, Harrison N, Simonet V, Zhitomirsky M E, Gvozdikova M V, Ziman T and Rønnow H M 2020 High field magnetization of FePS₃ Phys. Rev. B 101 024415
- [20] Dhakal R, Griffith S and Winter S M 2024 Hybrid spin-orbit exciton-magnon excitations in FePS₃ npj Quantum Mater. 9 64
- [21] Shekhter A, McDonald R, Ramshaw B and Modic K A 2023 Magnetotropic susceptibility *Phys. Rev. B* 108 035111
- [22] Nauman M 2024 Unpublished experimental data on $FePS_3$